

Lipid and metabolite profiles of human brain tumors by desorption electrospray ionization-MS

Alan K. Jarmusch^a, Valentina Pirro^a, Zane Baird^a, Eyas M. Hattab^b, Aaron A. Cohen-Gadol^c, and R. Graham Cooks^{a,1}

^aDepartment of Chemistry and Center for Analytical Instrumentation Development, Purdue University, West Lafayette, IN 47907; ^bDepartment of Pathology and Laboratory Medicine, Indiana School of Medicine, Indianapolis, IN 46202; and ^cDepartment of Neurological Surgery, Indiana University School of Medicine, Indianapolis, IN 46202

This contribution is part of the special series of Inaugural Articles by members of the National Academy of Sciences elected in 2015.

Contributed by R. Graham Cooks, December 21, 2015 (sent for review November 24, 2015; reviewed by Richard N. Zare and Arash Zarrine-Afsar)

Examination of tissue sections using desorption electrospray ionization (DESI)-MS revealed phospholipid-derived signals that differ between gray matter, white matter, gliomas, meningiomas, and pituitary tumors, allowing their ready discrimination by multivariate statistics. A set of lower mass signals, some corresponding to oncometabolites, including 2-hydroxyglutaric acid and *N*-acetyl-aspartic acid, was also observed in the DESI mass spectra, and these data further assisted in discrimination between brain parenchyma and gliomas. The combined information from the lipid and metabolite MS profiles recorded by DESI-MS and explored using multivariate statistics allowed successful differentiation of gray matter ($n = 223$), white matter ($n = 66$), gliomas ($n = 158$), meningiomas ($n = 111$), and pituitary tumors ($n = 154$) from 58 patients. A linear discriminant model used to distinguish brain parenchyma and gliomas yielded an overall sensitivity of 97.4% and a specificity of 98.5%. Furthermore, a discriminant model was created for tumor types (i.e., glioma, meningioma, and pituitary), which were discriminated with an overall sensitivity of 99.4% and a specificity of 99.7%. Unsupervised multivariate statistics were used to explore the chemical differences between anatomical regions of brain parenchyma and secondary infiltration. Infiltration of gliomas into normal tissue can be detected by DESI-MS. One hurdle to implementation of DESI-MS intraoperatively is the need for tissue freezing and sectioning, which we address by analyzing smeared biopsy tissue. Tissue smears are shown to give the same chemical information as tissue sections, eliminating the need for sectioning before MS analysis. These results lay the foundation for implementation of intraoperative DESI-MS evaluation of tissue smears for rapid diagnosis.

ambient ionization | MS imaging | multivariate statistics | pathology | neurosurgery

MS is increasingly being used in medicine (e.g., in clinical chemistry, pharmaceutical development, and proteomics). Ambient ionization methods generate ions under atmospheric conditions, with minimal to no sample preparation (1). Desorption electrospray ionization (DESI), an ambient method that uses a spray of charged solvent as the projectile, provides rapid chemical information while preserving tissue and cellular morphology, allowing subsequent histopathology on the same specimen (2). This feature allows integration of DESI-MS into current workflows and postacquisition pathology. DESI-MS has been used to study prostate cancer (3), bladder cancer (4), kidney cancer (5), seminoma (6), lymphoma (7), gastrointestinal cancer (8), and others. In each case, the recorded pattern of lipid signals allows the differentiation of cancer from normal tissue. DESI-MS has been previously used to explore chemical differences among glioma subtypes, grades, and tumor cell concentrations (relative percentage of tumor compared with parenchyma) (9, 10). Meningiomas have also been studied previously and were distinguished from normal dura mater (11).

The incidence of brain tumors is approximately the same as that of non-Hodgkin's lymphoma, melanoma, and urinary bladder cancer in adults over 20 y of age, and it is even more prevalent

among children. Gliomas (30%), meningiomas (33%), and pituitary tumors (15%) account for the majority of brain tumors in adults (12). The brain parenchyma is comprised of glia (e.g., astrocytes and oligodendrocytes) and neurons. In many cases, surgical resection is the most effective treatment option; however, surgery must contend with the dilemma of maximizing tumor excision while minimizing unintended neurological deficits. MRI, a critical imaging method, aids in defining the location and size of the tumor (13). The nuclear spin of hydrogen is exploited by MRI, allowing visualization of different anatomical structures (e.g., T1-weighted MRI) or pathologies (e.g., T2-weighted and contrast-enhanced MRI). Additional information can be obtained by positron emission tomography, functional MRI, diffusion weighted imaging, fluid-attenuated inversion recovery, and magnetic resonance spectroscopic imaging (MRSI). Raman spectroscopy performed *in vivo* seeks to provide chemical information that allows rapid identification of cancerous tissue (14). Fluorescence imaging uses appropriate molecular labels to visualize tumors during surgery (15, 16). The information provided by these methods is used primarily to visualize the tumor and assist in surgical resection. Histopathology performed on frozen tissue sections and tissue smears is the most common source of important pathologic information, specifically the type of tumor (e.g., glioma) and grade (e.g., low grade), which is provided during surgery. This pathologic analysis is often repeated for infiltrative tumors to guide the extent of resection at the tumor margins. Currently, this information is obtained outside of the operating room, taking upward of 20 min per sample and prolonging surgery. Histopathology relies heavily on morphologic and cytologic features revealed by staining of

Significance

Brain tumors can lead to a significant source of morbidity and mortality. The primary treatment is microsurgical resection, and the extent of resection is associated with length of survival. Unfortunately, reliable intraoperative tools for diagnosis and safe maximal resection of the tumor mass are lacking. Mass spectra (lipid and metabolite profiles) can be used to distinguish between healthy and diseased tissues by comparison of patterns of peak intensities using multivariate statistics. This experiment can be done on a timescale amenable to intraoperative analysis using tissue smears. These data can provide surgeons with near real-time pathologic information and guide the intraoperative resection of the tumor at the difficult to detect peritumoral borders.

Author contributions: A.K.J., V.P., and R.G.C. designed research; A.K.J., V.P., Z.B., E.M.H., and A.A.C.-G. performed research; A.K.J. and V.P. analyzed data; and A.K.J., V.P., Z.B., E.M.H., A.A.C.-G., and R.G.C. wrote the paper.

Reviewers: R.N.Z., Stanford University; and A.Z.-A., University of Toronto.

The authors declare no conflict of interest.

¹To whom correspondence should be addressed. Email: cooks@purdue.edu.

This article contains supporting information online at www.pnas.org/lookup/suppl/doi:10.1073/pnas.1523306113/-DCSupplemental.

cellular structures (e.g., nucleus and cytoplasm). However, brain tumors exhibit large genetic variability and genomic instability, which remain invisible to microscope-based pathology. Auxiliary testing, frequently immunohistochemistry or genetic sequencing, supports pathologic diagnosis and has been used to estimate treatment response (as in pharmacogenomics). Genetic testing remains time-consuming [reporting of isocitrate dehydrogenase (IDH) mutation status, a prognostic marker, can take weeks], creating delay in pathologic diagnosis and rendering treatment. However, recently, Shankar et al. (17) reported a genotyping method for IDH and telomerase reverse transcriptase mutations, with results available in 60 min.

Previous studies (3–11) have shown tissue discrimination by mass spectral profiles (m/z values and associated abundances) characteristic of different tissue types, including different disease states. Rapid and direct analysis of tissue provides molecular information on multiple compounds and is obtained on a time-scale of seconds to a few minutes. In this way, ambient ionization MS profiling stands in stark contrast to “-omics” techniques, which are based on separation (e.g., liquid chromatography) before MS and in which complex samples are extensively processed (e.g., by desalting, extraction, and derivatization) to reveal, in detail, the particular compounds present. Both the time required for analysis and the complexity of high-performance hyphenated MS systems mean that they are not amenable to intraoperative use.

The potential diagnostic value of using ambient ionization and MS profiles, especially those based on lipids (18), is increasingly being recognized as reflected by a growing number of studies. Detection of metabolites by ambient ionization has also proven useful in the detection of genetic mutations, such as IDH, but it remains underexplored for potential diagnostic value. Differences in the lipid composition of renal cell carcinoma (19) and colon cancer (20) from their respective normal parenchyma were detected by positive ion probe electrospray ionization-MS. Touch spray, a probe method allowing user-guided sampling, serves to differentiate prostate cancer from normal tissue based on glycerophospholipid distributions (3). Similar methods of ionization have been used for the detection of lipids from lung (21) and brain cancer (22). DESI-MS imaging of stereotactically registered brain tumor samples (23) gave results that correlated with histopathology and illustrated the potential for determining tumor cell concentration near the resection margins (10). The analysis of gastric cancer surgical margins has been reported recently, including pixel by pixel classification of heterogeneous tissue sections (8). Brain and other cancers have been investigated using rapid evaporative ionization-MS, a method that provides lipid-based differentiation between cancerous and normal tissue and has been performed in vivo on patients undergoing surgical resection with promising results; however, electrocauterization is destructive and should be used with discretion (24). Establishing a robust classification method is of vital importance and best implemented by including normal tissue. Obtaining normal tissue is particularly difficult in the case of brain tumors, in which absolute normal rarely exists for scientific study. Currently, intraoperative DESI-MS analysis is limited by the need for freezing and cryosectioning before analysis; therefore, we describe the use of tissue smears as a means to quickly acquire differentiating chemical information. There is little doubt that development of molecular techniques that rapidly discriminate cancerous tissue would be of great benefit to supplement intraoperative decision-making and pathologic evaluation.

Results and Discussion

DESI-MS Imaging of Human Brain Tissue Sections. We explore the chemical information obtained from banked frozen brain tissue sections by DESI-MS performed in the imaging mode. Negative ionization DESI-MS images were recorded using different MS tune methods consecutively from the same tissue section. The main features of the MS profiles in the ranges m/z 200–1,000 and

m/z 80–200 were found to be associated with glycerophospholipids and metabolites, respectively, and are referred to throughout as the lipid and the metabolite profiles, respectively. These two MS profiles, containing many ions with relative abundances characteristic of tissue type, were evaluated separately and also, together by data fusion. Appropriate selection of the DESI-MS solvent allowed acquisition of multiple images from the same tissue section while preserving tissue morphology for subsequent histopathology, allowing correlation of chemical, spatial, and pathologic information (2).

Differentiation of Gliomas and Brain Parenchyma. The chemical differences between brain parenchyma and gliomas were explored by comparing the molecular information obtained in the two MS profiles and evaluating their ability in differentiating disease state (i.e., normal vs. tumor). DESI-MS imaging revealed that gray and white matter mass spectra differ and could be defined spatially (*SI Appendix, Fig. S1*); however, areas of mixed composition were also noted. Gray matter (Fig. 1*A*) is comprised of glia and mostly unmyelinated neurons, and it is associated with a very abundant peak at m/z 834 identified by high-resolution MS and MS/MS fragmentation as phosphatidylserine (PS) with 40 carbons with 6 units of unsaturation (40:6); predominant acyl chains are 18:0 (stearic acid) and 22:6 (docosahexaenoic acid) as indicated by MS/MS (*SI Appendix, Fig. S2*). White matter (Fig. 1*B*) is characterized by an increased relative abundance of m/z 788 (PS 18:1–18:0), 888, 906, and 916. Sulfatides [e.g., m/z 888; (3'-sulfo)GalCer 24:1] are particularly abundant, which correlates with the increased myelination of neurons. The pattern of ions that corresponded to gray and white matter was consistent with previous studies of murine brain tissue (25). The variations seen in the ratio of the signals associated with m/z 834 and 888 do not compromise the differences in relative abundance between gray and white matter (*SI Appendix, Fig. S4*). Additional information on the identification of ions detected in the lipid profile can be found in *SI Appendix (SI Appendix, Figs. S2 and S3 and Table S1)*. Differences in the lipid profiles were noted between anatomical regions of the brain, such as the molecular layer of the cortex and the other cortical layers (e.g., in the specimen shown in *SI Appendix, Fig. S5*). The m/z 788, 834, and 885 varied between the molecular layer, which surrounds a meningeal blood vessel (apparent in the ion image of m/z 788) and that of the cortex itself. Furthermore, unsupervised multivariate analysis by interactive brushing (26) supports the observed differences. Specific cases of special pathological or chemical interest like this one are discussed throughout. The average mass spectrum for gliomas (Fig. 1*C*) is very different from that of normal brain parenchyma, in that it lacks the ions at m/z 834 and 888 characteristic of gray and white matter, respectively. Rather, an increase in the abundance of m/z 794 [chloride adduct of phosphatidylcholine (PC) 34:1] and m/z 885 [phosphatidylinositol (PI) 18:0_20:4] was noted.

Principal component analysis (PCA) was performed on the lipid profiles selected from pathology-defined regions of brain parenchyma and glioma tissue sections (Fig. 1*D* and *E*). Gray and white matters were well-separated based primarily on m/z 834 and 888, respectively. The dispersed locations of a few gray and white matter points, those that fall between their respective groupings, corresponded to tissue of mixed composition as reflected in the mass spectra (*SI Appendix, Fig. S6*). This observation reflects typical parenchyma composition, which contains a mixture of unmyelinated and myelinated neurons as well as glial cells. Brain parenchyma and glioma were well-separated in PCA space, indicating that the first level of pathologic evaluation (is this a glioma or brain parenchyma?) can be answered readily. Interestingly, the glioma grouping was dispersed (Fig. 1*D*). Dispersion along the vector of gray and white matter separation (right to left) is related to the relative contribution of the parenchyma background to the detected lipid profile. Specimen 42 (secondary infiltrated; with ~40% tumor cell concentration) is illustrative of the juxtaposition

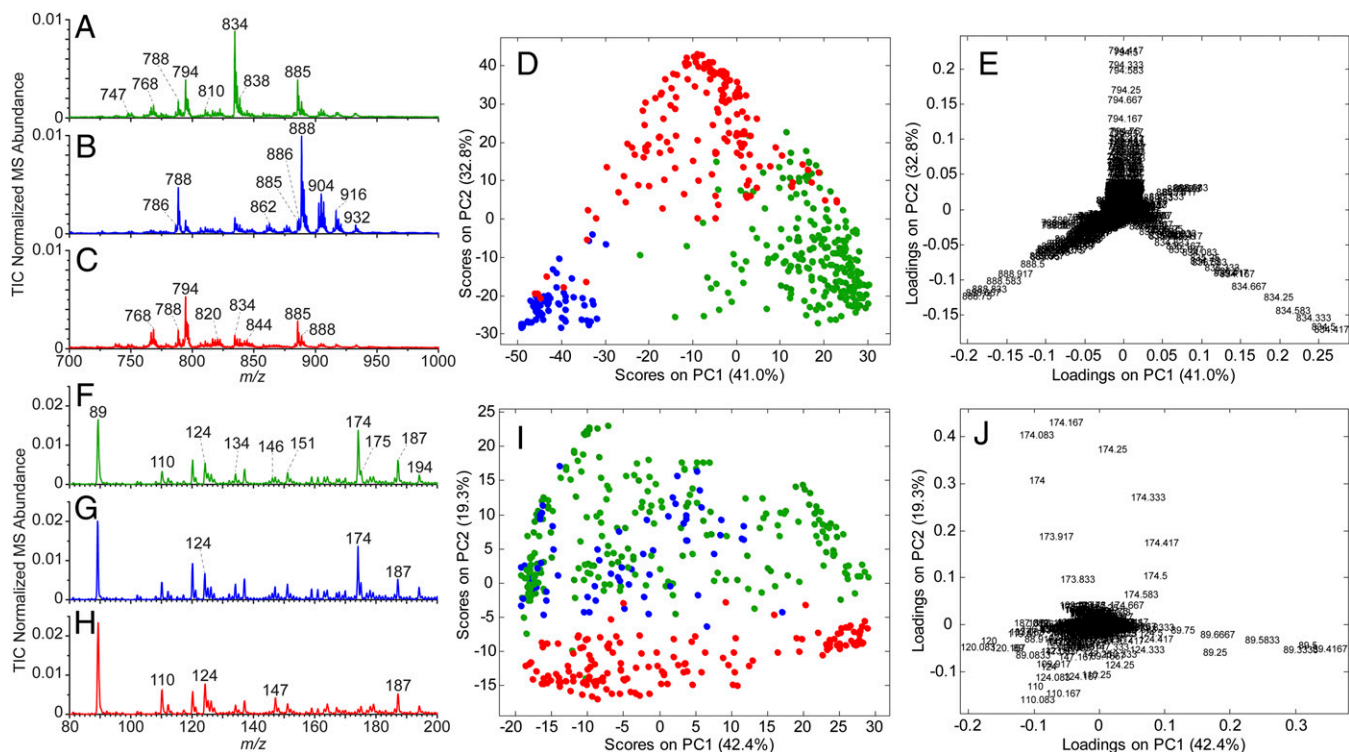


Fig. 1. Average lipid (m/z 700–1,000) and metabolite (m/z 80–200) MS profiles for gray matter ($n = 223$), white matter ($n = 66$), and glioma ($n = 158$) with PCA score and loading plots. Average normalized [total ion chromatogram (TIC)] lipid MS profile for (A) gray matter, (B) white matter, and (C) glioma. (D) PCA score plot [principal component 1 (PC1) vs. principal component 2 (PC2)] using lipid profile information for gray matter (green circles), white matter (blue circles), and glioma (red circles). (E) PCA loading plot with m/z annotated. Average metabolite MS profile for (F) gray matter, (G) white matter, and (H) glioma. (I) Metabolite profile PCA score plot for gray matter, white matter, and glioma and (J) corresponding PCA loading plot.

of gray and white matter regions (*SI Appendix, Figs. S7 and S8*) and the contribution of the background parenchyma to the lipid profile. The differences between gray and white matter can overshadow more subtle differences that indicate the presence of invasive tumor cells. This observation does not preclude the differentiation of normal tissue, infiltration, and gliomas but rather, confirms the complexity associated with brain tumors. The dispersion of the glioma class in the vertical direction in PCA score space (Fig. 1D) reflects the extent of infiltration of tumor cells. A likely contribution to the observed dispersion of the glioma group is the presence of glioma subtypes (e.g., astrocytoma and oligodendroglioma), which are related to the glial cells from which the cancer is derived. For example, the lipid profile of an oligodendroglioma might appear more similar to white matter, which is composed of a greater number of oligodendrocytes than gray matter. Discrimination of glioma subtypes has been previously studied (9) and is outside the scope of this study. Note that subsequent histopathologic evaluation revealed that normal specimens commonly contained various levels of secondary infiltration. The gray and white matter classes were comprised of regions containing <25% tumor cell concentration (mode was 10%), and one sample contained 40% tumor cell, representing a tissue composition that is reasonably expected near the surgical margin. A few samples well-separated from the glioma class in PCA space were considered completely normal and found by the pathologist to contain no observable tumor cells (<5%). Glioma points that fell between the glioma group and either the gray or white matter group illustrate the disease spectrum and the complexity in determining the disease state with contributions of background parenchyma and infiltration.

The metabolite profile, acquired subsequent to the lipid profile, has not been explored previously by DESI-MS in human brain tissue. The average metabolite profile mass spectra obtained from gray

matter, white matter, and gliomas are displayed in Fig. 1F–H, respectively. The anion of lactic acid was detected at m/z 89 (identified by exact mass measurements) (*SI Appendix, Fig. S9 and Table S1*) and occurred in slightly increased abundance ($128.9 \pm 17.5\%$) in gliomas vs. healthy tissue. This observation is consistent with metabolic aberrations inherent in cancer (e.g., high rates of aerobic glycolysis) as postulated by Warburg (27), but it does not seem to be uniquely predictive of disease. By contrast, a dramatic decrease in m/z 174 was noted between gray and white matter and gliomas. A box and whisker plot (Fig. 2A) indicated that m/z 174 alone allows discrimination of brain parenchyma from glioma (Kruskal–Wallis P value <0.001). Furthermore, a receiver-operating characteristic curve of brain parenchyma and glioma resulted in an area under the curve of 0.998 (*SI Appendix, Fig. S10*). Exact mass (Fig. 2B) and MS/MS fragmentation obtained by collision-induced dissociation (Fig. 2C) were used to identify m/z 174 as *N*-acetyl-aspartic acid (NAA) detected as the deprotonated ion. The dramatic difference between gray matter and glioma tissue is illustrated in specimen 51 (Fig. 2D). The intensities of m/z values 174, 794, 834, and 888 are plotted from individual pixels noted in Fig. 2E over the transition region from glioma to gray matter (Fig. 2F). The changes in the lipid ions correctly reflect the regions indicated as glioma and brain parenchyma by pathology (*SI Appendix, Fig. S11*). The change in NAA is evident with a similar rate of change to the lipids near the boundary of the two regions (approximately at pixel 12).

PCA was performed on the metabolite profile (Fig. 1I and J) and yielded poor separation of gray and white matter from each other but clear separation between brain parenchyma and glioma. The overwhelming significance of NAA in the multivariate separation is notable. Interestingly, this finding supports previous MRSI studies that indicated the significance of NAA in discriminating normal and diseased neural tissues (28, 29) and current use in

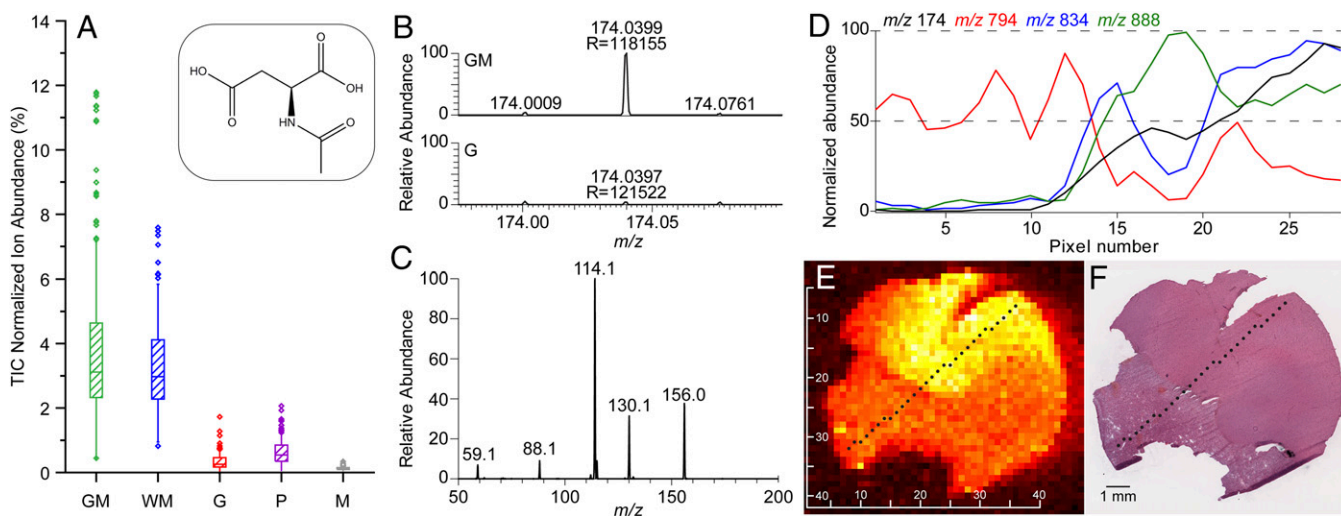


Fig. 2. Statistical significance and identification of NAA. (A) Box and whisker plot for m/z 174: gray matter (GM), $n = 223$; white matter (WM), $n = 66$; glioma (G), $n = 158$; pituitary (P), $n = 154$; and meningioma (M), $n = 111$. The box represents the interquartile range with a median line and whiskers ± 1.5 SD; outliers are represented by open circles. (A, Inset) NAA. (B) Detection of NAA by high-resolution MS in (Upper) gray matter and (Lower) high-grade glioma in specimen 51; m/z and resolution are annotated. (C) Collision-induced dissociation (CID) MS/MS fragmentation pattern obtained for NAA from gray matter in specimen 51. (D) Plot of intensity change of select ions [m/z 174 (black), 794 (red), 834 (blue), and 888 (green)] occurring with the transition between high-grade glioma and brain parenchyma in specimen 51. The pixels plotted in D (those of the horizontal scale bar) are indicated in the false-color image of a summed set of ions (281, 303, 788, 834, 885, and 888) in E. (F) H&E image of specimen 51 with approximate location of pixels.

tumor diagnosis (13, 30). However, detection of NAA in situ by MS has greater molecular specificity and speed compared with MRSI. NAA is an abundant molecule in the human nervous system, the biological function of which is still to be unraveled, but evidence indicates a significant role in neural metabolism (31). Ties to central metabolic processes can be made by aspartic acid as well as acetate, including lipid metabolism, energy production, amino acid synthesis, and gene regulation (31). Furthermore, NAA has been found to decrease in many neurological diseases and disorders, such as stroke, Alzheimer's disease, epilepsy, and multiple sclerosis (31). A reduction in the relative abundance of NAA was also noted in specimens containing reactive matter (SI Appendix, Fig. S12); thus, NAA seems to be an important measure of overall neural health.

2-Hydroxyglutaric acid (2HG; m/z 147) was also detected in the metabolite profile in some of the glioma samples. 2HG is a downstream metabolite of IDH mutations and serves as an important prognostic indicator (32, 33). The presence of m/z 147 in specimen 51 was confirmed by MS/MS (SI Appendix, Fig. S13) and found to correlate with the pathologically determined IDH mutation status. The presence of m/z 147 in the metabolite profile (full-scan mode) was indicative of 2HG presence, but additional specificity and confirmation were achieved by MS/MS. The detection of 2HG and its correlation with IDH mutation status are outside the scope of this report, having been investigated previously (33). The ability to ascertain such information rapidly expands the value of DESI-MS methodology beyond tissue diagnosis.

The best separation of gray and white matter and glioma was obtained when the lipid and metabolite profiles were considered together using midlevel data fusion (SI Appendix, Fig. S14). Gray matter ($n = 223$), white matter ($n = 66$), and gliomas ($n = 158$) were well-separated and had little intraclass dispersion. PCA followed by linear discriminant analysis (LDA) was performed to estimate classification performance when fusing the two MS profiles. The classification of gray matter, white matter, and gliomas (SI Appendix, Table S2) had an overall sensitivity (i.e., measure of the proportion of positives that are correctly identified as such) of 97.4% and a specificity (i.e., measure of the proportion of negatives that are correctly identified as such) of 98.5%. The methodology developed was further evaluated by predicting the

disease state and estimating the tumor cell concentration of a pathologically ambiguous specimen (Fig. 3) as an external validation. A false-color plot of the PC1 scores of individual pixels (SI Appendix, Fig. S15) revealed a region associated with glioma (red pixels in Fig. 3A) and a region more closely associated with white matter (blue pixels in Fig. 3A). Pathologic evaluation (Fig. 3B) of these two regions was ambiguous, with one clearly a glioma and the other being either a diffuse glioma or an infiltrated region adjacent to the tumor region, qualitatively matching our findings of two chemically different regions. Additional evaluation was performed using PCA LDA as shown in Fig. 3C, which classified a region of glioma (on the right in Fig. 3C) while classifying the adjacent region as white matter (on the left in Fig. 3C). The region classified by LDA as white matter prompted additional examination for infiltration (because infiltration was not a part of the PCA LDA model) by estimation of the tumor cell concentration. The tumor cell concentration of each pixel (Fig. 3D) was calculated by regression of a semilogarithmic plot of the natural log of NAA's TIC normalized abundance vs. tumor cell concentration (Pearson's $r = -0.89$) (SI Appendix, Fig. S15). The estimated tumor cell concentration in the glioma region was $>75\%$, whereas the other region had estimated concentrations ranging from $\sim 50\%$ to 30% , roughly matching with pathologic evaluation of 60% . This illustrative example supports that MS profiles, processed using multivariate statistics, can correctly discriminate gliomas and that they can also be used to detect diffuse and infiltrative tumors, a particularly critical question during surgical resection.

Discrimination of Tumor Types. Meningiomas and pituitary tumors represent a large fraction of all brain tumors; the lipid profile of the former was explored in a previous study (11). We sought to differentiate the tumor types investigated: glioma, meningioma, and pituitary tumor. The average lipid mass spectra displayed differences in the relative abundances of m/z 788, 794, and 885 between the tumor types (SI Appendix, Fig. S16). The metabolite profile, previously discussed as being highly significant for glioma discrimination, was less informative for meningiomas and pituitary tumors, with small changes being noted in the average mass spectra. PCA performed on glioma ($n = 158$), meningioma ($n = 111$), and pituitary tumors ($n = 154$) using the lipid information

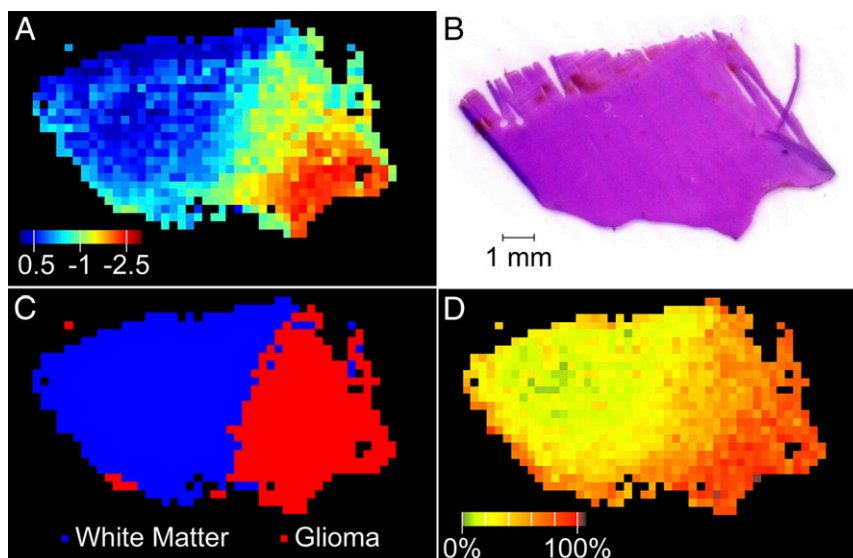


Fig. 3. DESI-MS predictions for specimen 65 and corresponding H&E. (A) PCA projection (false color) indicates PC1 score values. (B) H&E stain. (C) PCA LDA prediction of class and (D) calculated tumor cell concentration based on NAA abundance.

provided good separation between all tumor types and was supported by PCA LDA estimation of sensitivity (99.4%) and specificity (99.7%) (*SI Appendix, Table S3*). Although remarkable, this result is not surprising, because the cells and tissue from which the various tumors arise are quite different (e.g., glia vs. meninges), which is also reflected in histopathologic evaluation. The midlevel fusion of metabolite and lipid profile information did not substantially change the predicted classification. However, the average metabolite MS for meningiomas indicated the lowest amounts of m/z 89 (lactic acid) and 174 (NAA). In the case of NAA, the absence is supported by previous NMR and liquid chromatography-MS studies (34), thus serving as an endogenous positive control (i.e., signal neither expected nor detected). DESI-MS ion images of specimen 20 (*SI Appendix, Fig. S17*) illustrate the considerable difference between gray matter and an invasive boundary of a meningioma. Differential levels of NAA in gliomas, meningiomas, and pituitary tumors were reported by MRSI, and our data support these previous findings (29) (Fig. 2A). NAA signals were significantly different between tumor types ($P < 0.001$), although the lack of significant change (such as that observed between normal brain parenchyma and glioma) limits the predictive value of NAA for discriminating between tumor types. Comprehensively, lipid and metabolite profiles subjected to PCA yielded separation of gliomas, meningiomas, and pituitary tumors with little ambiguity, suggesting that an unknown sample from one of these three types of tumor could be chemically recognized by the MS profiles.

DESI-MS Imaging and Characterization of Human Brain Tissue Smears.

DESI-MS analysis of tissue smears is an attractive alternative to the use of tissue sections, removing the need for tissue freezing and sectioning. To date, DESI-MS analysis of tissue and cytological smears has been only briefly explored (7, 33). Smears are commonly performed by placing a minute amount of tissue onto a glass slide and then physically spreading the material to achieve a relatively uniform and diffuse layer of cellular material for staining and subsequent pathology. Smears are typically made using less than 50 mm³ tissue. A custom tissue smear device was designed to confine the tissue to the middle of the glass slide (along the narrowest dimension) and smear the tissue along the longest dimension with an approximate thickness of 100 μ m (*SI Appendix, Fig. S18*).

Tissue smears were imaged over an area of ~ 75 mm², exploring the MS quality and the homogeneity of the chemical information. The absolute MS signal was generally equal to that of tissue sections. Importantly, the relative abundances of the ions were similar between tissue sections and tissue smears. The average metabolite and lipid profiles of gray matter and gliomas (*SI Appendix, Fig. S19*) mirror those of the tissue sections. For example, the abundance of m/z 834 is notable in the gray matter spectrum and dramatically reduced in the gliomas. Similarly, the statistical significance of NAA (m/z 174; $P < 0.001$) allows for the discrimination of gray matter and gliomas (*SI Appendix, Fig. S20*). Canonical correlation analysis (CCA) (35) was performed to assess the similarity of the chemical information obtained from tissue smears and sections (*SI Appendix, Fig. S21*). The correlation coefficients are notable (greater than 0.95) between the first three canonical variables for both the lipid and metabolite profiles, emphasizing that the physical change induced by smearing does not influence the chemical information. As a precaution, it should be mentioned that the sample matrix and associated analytical effect could influence the data obtained by MS, but this effect was not observed in our experiments. The lipid and metabolite profiles of smears were nearly identical to those recorded from tissue sections, indicating that sectioning can be foregone for more rapid tissue smear analysis.

Conclusions

The application of DESI-MS in brain cancer resection requires knowledge of the characteristic chemical features that distinguish brain parenchyma from glioma and different tumor types from each other, and these differences are explored here for the first time to our knowledge. The strategy of using MS profiles to characterize tissue differs from the traditional use of biomarkers, in which a single molecule (or ion detected by MS) is used as an indicator of disease. MS profiles are an integrated representation of downstream metabolism and provide important information that extends beyond tissue diagnosis (e.g., in the case of 2HG to prognosis).

In this study, we show that MS analysis of tissue sections revealed lipid-derived and metabolite signals that differ between gray and white matter and gliomas, facilitating discrimination by multivariate statistics. Difference in the MS profiles revealed the effect of brain parenchyma on the signal obtained from glioma samples. This

observation is particularly significant, because gliomas frequently invade along white matter tracts, illustrating the need to understand the contribution of brain parenchyma and infiltration in predicting disease state. The significance of NAA in discriminating brain parenchyma and glioma is clear and immense. This study offers strong evidence that NAA is, in fact, an oncometabolite and the first in situ detection, to our knowledge, of NAA by ambient MS. The importance of NAA in glioma differentiation confirms nearly 20-y-old MRSI data. NAA also seems to be predictive of tumor cell concentration in unknown samples with an exponential-like decay in MS signal from brain parenchyma to glioma. Fusion of the lipid and metabolite MS profiles provided the best discrimination of brain parenchyma (gray and white matter) and gliomas, with an overall sensitivity of 97.4% and a specificity of 98.5%. Furthermore, the MS profiles proved capable of discriminating tumor types (i.e., glioma, meningiomas, and pituitary tumors) with sensitivity and specificity >99%.

Surgical intervention of brain tumors could be simplified with intraoperative analysis of tissue without extending operative times. Tissue smears that eliminate the need for tissue freezing and sectioning before DESI-MS were explored. The use of a custom 3D-printed smear device aided in the distribution of tissue during smearing while maintaining a sufficiently thin smear for DESI-MS. The observed lipid or metabolite profiles were not significantly altered by the physical act of smearing, and their signal intensities were comparable with those of tissue sections. Furthermore, the chemical information obtained from tissue smears was equivalent to that from tissue sections as determined by CCA. The validation of tissue smears as samples for discriminative analysis remains to be

fully vetted; however, this work lays the foundation for implementation of DESI-MS intraoperatively.

Materials and Methods

Cryopreserved human neurological specimens were obtained from 74 patients (58 patients of whom were included in the sample cohort) through the Biorepository of Methodist Research Institute. Tissue specimens were prepared as tissue sections and tissue smears on glass microscope slides and stored at -80°C before analysis. MS measurements were performed on a linear ion trap mass spectrometer (Finnigan LTQ; Thermo Electron Corporation). High-resolution MS measurements were performed using an Orbitrap Mass Spectrometer (Exactone, Thermo). DESI-MS was performed using dimethylformamide-acetonitrile (1:1 vol/vol), which preserved tissue morphology for subsequent pathology. Blind histopathologic evaluation was performed by an expert pathologist. Sections and smears were subjected to two sequential negative-mode DESI-MS image acquisitions (250- μm pixel resolution). The first image included data from m/z 200–1,000, with the mass spectrometer tuned for maximum transmission of m/z 786. The moving stage was then reset to the origin position, allowing for a subsequent image was acquired from m/z 80–200 (MS tuned for m/z 174). Data were exported from XCalibur 2.0 into .csv files, which were then imported into MATLAB. In-house MATLAB routines were used to process all MS data unless otherwise specified. Multivariate statistics, including PCA, midlevel data fusion PCA, and CCA, were performed on the data. Kruskal–Wallis nonparametric test was used to evaluate the statistical significance of NAA. Additional information and discussion of the materials and methods can be found in *SI Appendix*.

ACKNOWLEDGMENTS. The authors thank the Purdue University for Cancer Research, Clint Alfaro, Paolo Oliveri, Cody Howell, and George Sandusky. Research was supported by National Institute of Biomedical Imaging and Bioengineering of the NIH Grant R21EB015722. V.P. thanks the American Society for Mass Spectrometry (ASMS) for a 2015 ASMS Post-Doctoral Award.

- Domin M, Cody R, eds (2014) *Ambient Ionization Mass Spectrometry* (Royal Society of Chemistry, Cambridge, United Kingdom).
- Eberlin LS, et al. (2011) Nondestructive, histologically compatible tissue imaging by desorption electrospray ionization mass spectrometry. *ChemBioChem* 12(14):2129–2132.
- Kerian KS, et al. (2015) Differentiation of prostate cancer from normal tissue in radical prostatectomy specimens by desorption electrospray ionization and touch spray ionization mass spectrometry. *Analyst (Lond)* 140(4):1090–1098.
- Dill AL, et al. (2011) Multivariate statistical identification of human bladder carcinomas using ambient ionization imaging mass spectrometry. *Chemistry* 17(10):2897–2902.
- Dill AL, et al. (2010) Multivariate statistical differentiation of renal cell carcinomas based on lipidomic analysis by ambient ionization imaging mass spectrometry. *Anal Bioanal Chem* 398(7–8):2969–2978.
- Masterson TA, et al. (2011) Distinctive glycerophospholipid profiles of human seminoma and adjacent normal tissues by desorption electrospray ionization imaging mass spectrometry. *J Am Soc Mass Spectrom* 22(8):1326–1333.
- Jarmusch AK, et al. (2015) Characteristic lipid profiles of canine non-Hodgkin's lymphoma from surgical biopsy tissue sections and fine needle aspirate smears by desorption electrospray ionization–mass spectrometry. *Analyst (Lond)* 140(18):6321–6329.
- Eberlin LS, et al. (2014) Molecular assessment of surgical-resection margins of gastric cancer by mass-spectrometric imaging. *Proc Natl Acad Sci USA* 111(7):2436–2441.
- Eberlin LS, et al. (2012) Classifying human brain tumors by lipid imaging with mass spectrometry. *Cancer Res* 72(3):645–654.
- Eberlin LS, et al. (2013) Ambient mass spectrometry for the intraoperative molecular diagnosis of human brain tumors. *Proc Natl Acad Sci USA* 110(5):1611–1616.
- Calligaris D, et al. (2015) Molecular typing of meningiomas by desorption electrospray ionization mass spectrometry imaging for surgical decision-making. *Int J Mass Spectrom* 377:690–698.
- Ostrom QT, et al. (2014) CBRUS statistical report: Primary brain and central nervous system tumors diagnosed in the United States in 2007–2011. *Neuro-oncol* 16(Suppl 4):iv1–iv63.
- Kwock L (2014) *Proton Magnetic Resonance Spectroscopy and Spectroscopic Imaging of Primary Brain Tumors. Functional Brain Tumor Imaging* (Springer, Berlin), pp 143–167.
- Jermyn M, et al. (2015) Intraoperative brain cancer detection with Raman spectroscopy in humans. *Sci Transl Med* 7(274):274ra19.
- Pogue BW, et al. (2010) Review of neurosurgical fluorescence imaging methodologies. *IEEE J Sel Top Quantum Electron* 16(3):493–505.
- van Dam GM, et al. (2011) Intraoperative tumor-specific fluorescence imaging in ovarian cancer by folate receptor- α targeting: First in-human results. *Nat Med* 17(10):1315–1319.
- Shankar GM, et al. (2015) Rapid intraoperative molecular characterization of glioma. *JAMA Oncol* 1(5):662–667.
- Barceló-Coblijn G, Fernández JA (2015) Mass spectrometry coupled to imaging techniques: The better the view the greater the challenge. *Front Physiol* 6(3):3.
- Yoshimura K, et al. (2012) Analysis of renal cell carcinoma as a first step for developing mass spectrometry-based diagnostics. *J Am Soc Mass Spectrom* 23(10):1741–1749.
- Mandal MK, et al. (2013) Biomolecular analysis and cancer diagnostics by negative mode probe electrospray ionization. *Analyst (Lond)* 138(6):1682–1688.
- Wei Y, et al. (2015) Tissue spray ionization mass spectrometry for rapid recognition of human lung squamous cell carcinoma. *Sci Rep* 5(2015):10077.
- Kononikhin A, et al. (2015) A novel direct spray-from-tissue ionization method for mass spectrometric analysis of human brain tumors. *Anal Bioanal Chem* 407(25):7797–7805.
- Agar NY, et al. (2011) Development of stereotactic mass spectrometry for brain tumor surgery. *Neurosurgery* 68(2):280–289.
- Balog J, et al. (2013) Intraoperative tissue identification using rapid evaporative ionization mass spectrometry. *Sci Transl Med* 5(194):194ra93.
- Eberlin LS, Ifa DR, Wu C, Cooks RG (2010) Three-dimensional visualization of mouse brain by lipid analysis using ambient ionization mass spectrometry. *Angew Chem Int Ed Engl* 49(5):873–876.
- Pirro V, Eberlin LS, Oliveri P, Cooks RG (2012) Interactive hyperspectral approach for exploring and interpreting DESI-MS images of cancerous and normal tissue sections. *Analyst (Lond)* 137(10):2374–2380.
- Warburg O (1956) On the origin of cancer cells. *Science* 123(3191):309–314.
- Preul MC, et al. (1996) Accurate, noninvasive diagnosis of human brain tumors by using proton magnetic resonance spectroscopy. *Nat Med* 2(3):323–325.
- Kinoshita Y, Yokota A (1997) Absolute concentrations of metabolites in human brain tumors using in vitro proton magnetic resonance spectroscopy. *NMR Biomed* 10(1):2–12.
- Soares DP, Law M (2009) Magnetic resonance spectroscopy of the brain: Review of metabolites and clinical applications. *Clin Radiol* 64(1):12–21.
- Moffett JR, Ross B, Arun P, Madhavarao CN, Namboodiri AM (2007) N-Acetylaspartate in the CNS: From neurodiagnostics to neurobiology. *Prog Neurobiol* 81(2):89–131.
- Dang L, et al. (2009) Cancer-associated IDH1 mutations produce 2-hydroxyglutarate. *Nature* 462(7274):739–744.
- Santagata S, et al. (2014) Intraoperative mass spectrometry mapping of an oncometabolite to guide brain tumor surgery. *Proc Natl Acad Sci USA* 111(30):11121–11126.
- Urenjak J, Williams SR, Gadian DG, Noble M (1992) Specific expression of N-acetylaspartate in neurons, oligodendrocyte-type-2 astrocyte progenitors, and immature oligodendrocytes in vitro. *J Neurochem* 59(1):55–61.
- Doeswijk T, et al. (2011) Canonical correlation analysis of multiple sensory directed metabolomics data blocks reveals corresponding parts between data blocks. *Chemometr Intell Lab Syst* 107(2):371–376.